

Arbitrary Polarization Generation in Magneto-optical Metasurfaces Enabled by Bound States in the Continuum

SIYUAN GAO^{1,*}, GUANGTAI LU^{2,3}, SATOSHI IWAMOTO^{2,3}, AND YASUTOMO OTA^{1,*}

¹Department of Applied Physics and Physico-Informatics, Keio University, Japan

²Research Center for Advanced Science and Technology, The University of Tokyo, Japan

³Institute of Industrial Science, The University of Tokyo, Japan

*gaosy@keio.jp, ota@appi.keio.ac.jp

Compiled March 12, 2026

The generation of arbitrary polarization states of light is essential for optical communication and photonic information processing. Photonic crystal and metasurface platforms supporting bound states in the continuum (BICs) provide a powerful route for polarization engineering through tailoring the radiation from the resonant modes. However, existing approaches typically rely on static structural symmetry breaking or off-normal radiation, which limits continuous polarization tuning of vertical radiation. Here, we demonstrate a magneto-optical metasurface that generates arbitrary polarization states of light at normal radiation. By applying an external magnetic field with variable orientation, a symmetry-protected BIC is transformed into a quasi-BIC whose radiation polarization can be continuously tuned. The magneto-optical perturbation drives the controlled migration of polarization singularities in momentum space, allowing the emitted states to continuously span the entire Poincaré sphere without structural modification. This approach establishes a compact platform for actively tunable polarization sources and polarization-encoded photonic devices.

<http://dx.doi.org/10.1364/ao.XX.XXXXXX>

The generation of arbitrary states of polarization (SoP) for light offers new opportunities for optical communication networks [1, 2], photonic signal processing [3, 4] and polarization-encoded information technologies [5–8]. Conventionally, polarization control has been achieved using birefringent materials and anisotropic optical elements [9–11]. More recently, high-quality factor (Q) photonic platforms provide an effective route to polarization control via the manipulation of optical modes [12]. In particular, bound states in the continuum (BICs) found in periodic photonic crystals and metasurface structures have attracted considerable attention for polarization engineering [13–17]. BICs often emerge at polarization singularities in momentum space, which carry integer topological charges associated with vortex-like polarization textures [18–22]. The existence of such polariza-

tion singularities enables access to a wide variety of SoP through momentum space engineering.

A widely adopted strategy to manipulate polarization singularities is geometric symmetry breaking. By reducing the symmetry of the photonic structure, symmetry-protected BICs are transformed into quasi-BICs with finite quality factors (Q) [23, 24], accompanied by the splitting of vortex-type polarization singularities (V points) into circular polarization singularities (C points) [17, 25–27]. Such symmetry-controlled approaches have enabled access to various polarization states [28–31]. However, because the polarization response is directly tied to structural geometry, the achievable polarization states are fixed after fabrication, severely limiting its flexibility and reconfigurability.

To overcome the limits of fixed structure, external perturbations have been explored as a means of tuning BICs without modifying the structure [32–34]. Among them, the magneto-optical (MO) effect provides a particularly powerful approach. Previous studies have shown that MO effect can convert symmetry-protected BICs into radiative quasi-BICs [33, 35] and induce splitting and reconfiguration of polarization singularities in momentum space [36–44]. However, existing approaches primarily rely on off-normal radiation or provide access only to a limited subset of polarizations, preventing continuous and deterministic control of the SoP in vertical radiation.

In this work, we demonstrate an all-dielectric MO metasurface that enables continuous and complete control of the SoP radiated from the Γ point by manipulating the polarization singularity of the BIC mode without any structural modification. We manipulate the SoP through the azimuthal and elevation angles of the applied magnetic field, which independently control the orientation and ellipticity of the radiation. This approach establishes a high- Q platform for full-Stokes polarization control, overcoming the fundamental limitations of static symmetry breaking and off-axis radiation in previous BIC-based schemes.

Our design is based on the all-dielectric MO metasurface schematically shown in Fig. 1(a), consisting of a square array of MO nanorods suspended in air. The lattice constant is $a = 1000$ nm, the rod height $h = 1000$ nm, and the diameter $D = 800$ nm. The relative permittivity tensor of the MO material is

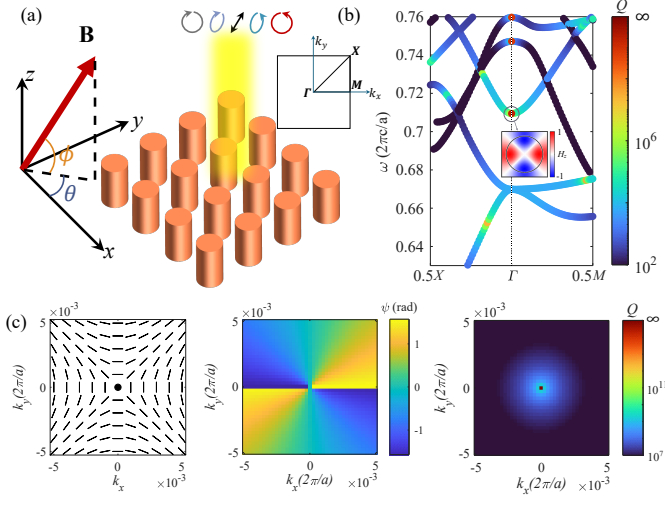


Fig. 1. (a) Schematic illustration of the MO metasurface and direction of external magnetic field. (b) Band diagram of the investigated structure, inset: Mode profile of the investigated BIC mode. (c) The map of polarization state, orientation angle ψ and Q factor of this TE band in momentum space without external magnetic field.

represented as follows[45]:

$$\hat{\varepsilon} = \begin{pmatrix} \varepsilon_x & -ig_z & ig_y \\ ig_z & \varepsilon_y & -ig_x \\ -ig_y & ig_x & \varepsilon_z \end{pmatrix} \quad (1)$$

where the diagonal components of the permittivity tensor are taken as $\varepsilon_x = \varepsilon_y = \varepsilon_z = 2.3^2$ without loss of generality. The MO response of the material is described by the off-diagonal part of the permittivity tensor denoted as g_i . Assuming a magnetic field with variable orientation, the MO constants are parameterized as

$$\begin{aligned} g_x &= g_0 \cos \theta \cos \phi \\ g_y &= g_0 \sin \theta \cos \phi \\ g_z &= g_0 \sin \phi \end{aligned} \quad (2)$$

where g_0 denotes the overall magnitude of the MO constant. θ and ϕ are the azimuthal angle and the elevation angle of the applied magnetic field. Numerical simulations of the eigenmodes and radiation properties are performed using the finite-element method implemented in COMSOL multiphysics. The momentum-resolved far-field radiation is obtained by projecting the Bloch eigenmode fields onto outgoing plane-wave components[18]. The state of polarization (SoP) is characterized using the orientation angle ψ and ellipticity angle χ , which are extracted from the Stokes parameters of the far-field electric field.

Firstly, we investigate the photonic band diagram in the absence of an external magnetic field ($g_0 = 0$) of the MO metasurface as illustrated in Fig. 1(b). Several symmetry protected BIC modes with infinitely high Q are observed at the Γ point. The mode of interest is the polarization-degenerate TE-like quadrupole resonance mode, whose magnetic field profile is illustrated in the inset. Next, we investigate the SoP and Q around the BIC point in momentum space as shown in Fig. 1(c). A polarization vortex composed of a linearly-polarized state is

observed around the Γ point, where the orientation angle (ψ) undergoes a change of -2π along a closed loop encircling the Γ point, indicating a topological charge of -1 [18]. Q factor diverges as the wave vector approaches the Γ point and decreases rapidly away from this highly symmetric point in the momentum space.

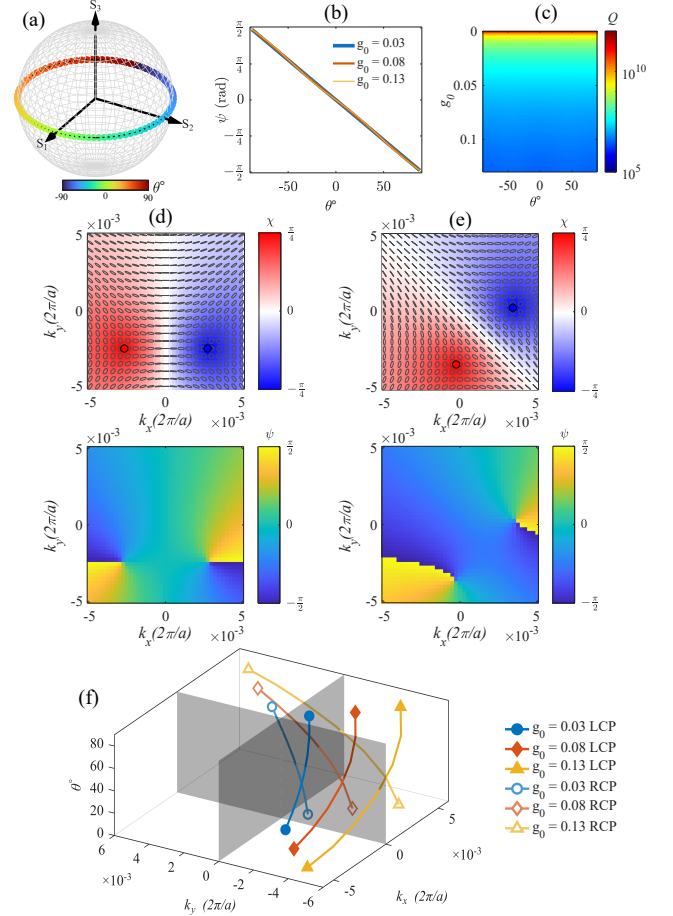


Fig. 2. In-plane MO effect and manipulation of SoP and Q of TE-mode at Γ point. (a) SoP at the Γ point plotted on the Poincaré sphere for $g_0 = 0.03$ and $\phi = 0^\circ$ as θ varying from -90° to 90° , showing a continuous sweep along the equator that covers all linear-polarization orientations; (b) Orientation angle ψ as a function of θ with $g_0 = 0.03, 0.08$ and 0.13 . (c) Q factor distribution with varying θ and g_0 . Polarization plot, χ and ψ distribution of TE quasi-BIC mode in momentum space with (d) $g_0 = 0.08, \phi = 0^\circ$ and $\theta = 0^\circ$ and (e) $g_0 = 0.08, \phi = 0^\circ$ and $\theta = 45^\circ$; (f) The movement trajectory of LCP and RCP point with increasing θ with $g_0 = 0.03, 0.08$ and 0.13 and $\phi = 0^\circ$.

We next examine the impact of the in-plane ($\phi = 0^\circ$) MO effect on the far field polarization at Γ point. The nonzero in-plane MO effect converts BIC modes to radiative modes with finite Q factors [33]. Fig. 2(a) plots the polarization states of the quasi-BIC mode at the Γ point on the Poincaré sphere for $g_0 = 0.03$ as the magnetization angle θ varies from -90° to 90° . The resulting states are continuously distributed along the entire equatorial line of the sphere, demonstrating that by altering θ , all possible orientation angle ψ from $-\frac{\pi}{2}$ to $\frac{\pi}{2}$ are generated. In addition, this indicates that the in-plane MO effect enables

complete coverage of the linear polarization manifold without introducing any circular component. The computed ψ varies linearly with θ and its slope is independent of g_0 , as shown in Fig. 2(b). In contrast, the corresponding Q , as shown in Fig. 2(c), decreases exponentially with increasing g_0 , but remains insensitive to θ . This shows that θ governs the polarization orientation ψ while g_0 controls the radiative leakage of the quasi-BIC modes at the Γ point.

To explore polarization behavior in momentum space, we map the far-field polarization distribution of the investigated TE-like eigenmodes with $g_0 = 0.08$. For $(\theta, \phi) = (0^\circ, 0^\circ)$, Fig. 2(d) reveals a pair of circular polarization singularities (C points) with opposite handedness located symmetrically about $k_x = 0$. The red and blue markers correspond to left (LCP) and right circular polarized (RCP) states ($\chi = \pm \frac{\pi}{4}$), respectively. The colormap of the orientation angle ψ exhibiting a phase winding of $-\pi$ and a topological charge of $-\frac{1}{2}$ at each C point. Along the symmetry line ($k_x = 0$), the polarization remains linear with $\psi = 0$, forming an L-line that divides the two C points [27]. When the magnetization is rotated to $\theta = 45^\circ$, as shown in Fig. 2(e), the C points shift diagonally together with the L line, and the linear-polarization axis at Γ rotates correspondingly to $\psi = -\frac{\pi}{4}$. The complete trajectories of the C points as a function of θ are summarized in Fig. 2(f). Increasing g_0 enlarges the separation between the C points, while changing θ induces their azimuthal rotation around Γ point. The in-plane magnetic field enabled the change of ψ by θ and independent tuning of Q by g_0 at the Γ point.

The effect of an out-of-plane magnetic field ($\phi \neq 0^\circ$) is investigated in Fig. 3. Fig. 3(a) compares the evolution of the state of polarization (SoP) at the Γ point under varying elevation angle ϕ for $g_0 = 0.03, 0.08$ and 0.13 , with the azimuthal angle fixed at $\theta = 0^\circ$. The SoPs are plotted on the Poincaré sphere, where the color scale denotes ϕ ranging from -89° to 89° . The case $\phi = 90^\circ$ is excluded, as it corresponds to a purely out-of-plane magnetization ($g_x = g_y = 0$), under which the symmetry-protected BIC at the Γ point is restored. For a weak MO constant ($g_0 = 0.03$), the SoP follows a near-vertical trajectory along the $S_2 = 0$ meridian, where the ellipticity χ increases gradually with increasing $|\phi|$. As g_0 increases to 0.08 , the trajectory extends toward the north and south poles ($S_3 = \pm 1$), reaching pure LCP and RCP states at $\phi = \pm 66.1^\circ$. Further increasing g_0 to 0.13 causes the trajectory to cross the poles at $\phi = \pm 34^\circ$ and continue into the opposite hemisphere. These results indicate that ϕ continuously controls the ellipticity through the S_3 component, while g_0 determines the accessible range of polarization states. Fig. 3(b) presents the ellipticity χ of the quasi-BIC mode at the Γ point as a function of ϕ and g_0 . The ellipticity χ evolves continuously in the (g_0, ϕ) parameter space. The white dashed curve denotes the iso-contour $\chi = \frac{\pi}{4}$, corresponding to a pure circular polarization state. To realize the pure circular state, the MO constant g_0 must be larger than 0.074 . Fig. 3(c) illustrates the corresponding Q of the QBIC mode at the Γ point as a function of g_0 and ϕ . The Q decreases with increasing g_0 or decreasing ϕ , reflecting enhanced radiative loss induced by symmetry breaking due to the MO effect. When ϕ reached 90° , the Q factor diverges again, indicating recovery of the symmetry-protected BIC at the Γ point.

The topological interpretation of pure circular SoP is confirmed in Fig. 3(d) for $g_0 = 0.08$ and $\phi = 66.1^\circ$, where the SoP map in momentum space shows that Γ point exhibits pure circular polarization ($\chi = \frac{\pi}{4}$) with half topological charge, while an opposite-handed C point appears at an off- Γ wave vector $(k_x, k_y) = (0.005 \frac{\pi}{a}, -0.004 \frac{\pi}{a})$. The corresponding orientation

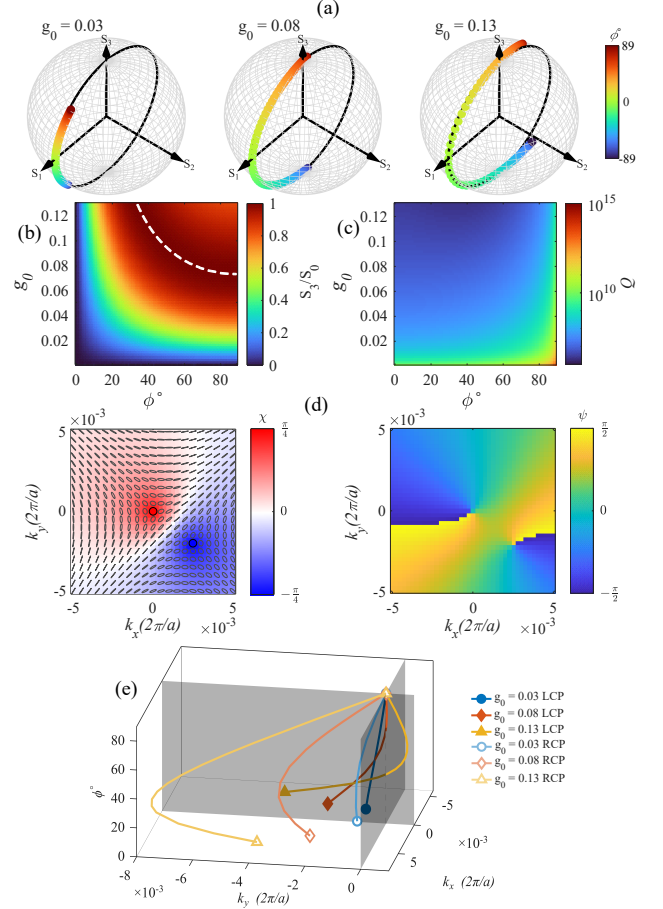


Fig. 3. Out-of-plane MO effect and manipulation of SoP and Q of TE-mode at Γ point. (a) SoP at the Γ point plotted on the Poincaré sphere for $g_0 = 0.03, 0.08$ and 0.13 as ϕ varying from -89° to 89° ; (b) Ellipticity χ distribution with varying ϕ ($0^\circ - 89^\circ$) and g_0 , the white dashed line is the iso-valued line presenting $\chi = \frac{\pi}{4}$; (c) Q factor distribution with varying ϕ ($0^\circ - 89^\circ$) and g_0 ; (d) Polarization plot, χ and ψ distribution in momentum space with $g_0 = 0.08$, $\phi = 66.1^\circ$ and $\theta = 0^\circ$; (e) The trajectory of LCP and RCP point with increasing ϕ with $g_0 = 0.03, 0.08, 0.13$ under $\theta = 0^\circ$.

map reveals half-integer topological charges associated with these points. Fig. 3(e) traces the full trajectories of the C points as ϕ increases from 0° to 90° . For a weak MO coupling strength ($g_0 = 0.03$), the LCP and RCP points approach each other and annihilate at the Γ point only when $\phi = 90^\circ$. For stronger coupling conditions ($g_0 = 0.08$ and 0.13), one of the C points crosses the Γ point at $\phi < 90^\circ$, giving rise to circularly polarized radiation with finite Q , before both C points annihilate again at $\phi = 90^\circ$. These results demonstrate that the emergence of circular polarization at the Γ point is governed by the out-of-plane component of the external magnetic field.

Finally, we demonstrate the generation of arbitrary SoP of the quasi-BIC mode at the Γ point by jointly tuning θ and ϕ under a fixed $g_0 = 0.08$. The parameters were swept over $\theta = [-90^\circ, 90^\circ]$ and $\phi = [-89^\circ, 89^\circ]$. The resulting polarization states, shown in Fig. 4(a), reveal that tuning θ continuously rotates the linear polarization orientation, while varying ϕ introduces and controls the circular component of the polarization. The $\chi = \frac{\pi}{4}$ is realized at $\phi = 66.1^\circ$. By combining both degrees

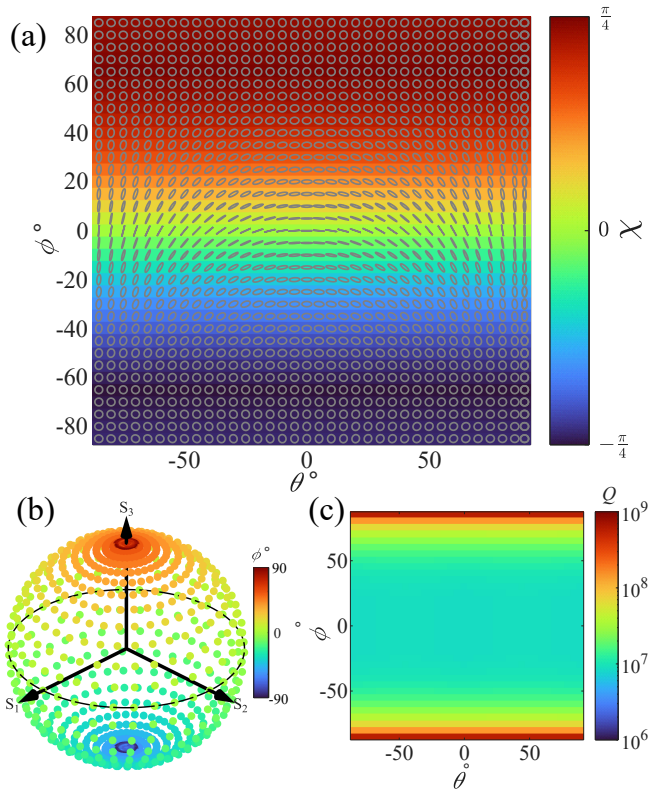


Fig. 4. Arbitrary polarization states control. The SoP at Γ point under different θ and ϕ , where polarization plot and colormap of ellipticity χ (rad) (a), the SOP plot on Poincaré sphere and the corresponding Q factor (c).

of freedom, the emitted SoPs can be tuned across all possible elliptical states, enabling full coverage of the Poincaré sphere as confirmed in Fig. 4(b). This demonstrates that the designed MO metasurface supports complete and continuous generation of arbitrary polarization states, from linear to elliptical to circular, using only the variation of the applied magnetic field. The corresponding map of Q at Γ point, as shown in Fig. 4(c), which can be tuned by changing the value of g_0 . These results establish a magnetically reconfigurable all-dielectric metasurface capable of deterministic and lossless polarization control at a single-frequency BIC resonance.

In summary, our simulations demonstrate that the application of an external magnetic field transforms the BIC mode into a radiative quasi-BIC mode whose polarization can be deterministically controlled solely by the magnetic field orientation. We identified that the elevation angle (ϕ) controls the polarization orientation (ψ) and the azimuthal angle (θ) controls the ellipticity (χ), while the strength of the MO effect (g_0) helps control Q factor. This work establishes a magneto-optical route toward all-dielectric metasurfaces capable of full Stokes-parameter control without structural modification. The demonstrated mechanism provides a compact and reconfigurable platform for next-generation photonic technologies.

Funding. This work was supported by JST FOREST (JPMJFR213F), JST CREST (JPMJCR19T1) and KAKENHI (25K01697, 24K17582), Iketani Foundation, Nippon Sheet Glass Foundation.

Disclosures. The authors declare no conflicts of interest.

REFERENCES

- W. Deng, L. Chen, H. Zhang, *et al.*, *Laser & Photonics Rev.* **16**, 2200136 (2022).
- C. Guo, F. Liu, S. Chen, *et al.*, *IEEE Commun. Surv. & Tutorials* **19**, 125 (2017).
- H. Kwon, D. Sounas, A. Cordaro, *et al.*, *Phys. Rev. Lett.* **121**, 173004 (2018).
- D. Gao, W. Ding, M. Nieto-Vesperinas, *et al.*, *Light. Sci. & Appl.* **6**, e17039 (2017).
- X. Li, T.-H. Lan, C.-H. Tien, and M. Gu, *Nat. Commun.* **3**, 998 (2012).
- Y. Lu, Z. Liao, and X.-H. Wang, *Phys. Rev. Lett.* **134**, 083601 (2025).
- J.-C. Boileau, D. Gottesman, R. Laflamme, *et al.*, *Phys. Rev. Lett.* **92**, 017901 (2004).
- Z. Zhan, M. Cantono, V. Kamalov, *et al.*, *Science* **371**, 931 (2021).
- S. Wang, Z.-L. Deng, Y. Wang, *et al.*, *Light. Sci. & Appl.* **10**, 24 (2021).
- E. W. Wang, S. Yu, T. Phan, *et al.*, *Laser & Photonics Rev.* **17**, 2200926 (2023).
- Z. Li, W. Liu, Y. Zhang, *et al.*, *Photonix* **5**, 30 (2024).
- J. P. Balthasar Mueller, N. A. Rubin, R. C. Devlin, *et al.*, *Phys. Rev. Lett.* **118**, 113901 (2017).
- C. W. Hsu, B. Zhen, A. D. Stone, *et al.*, *Nat. Rev. Mater.* **1** (2016).
- C. W. Hsu, B. Zhen, J. Lee, *et al.*, *Nature* **499**, 188 (2013).
- M. Kang, T. Liu, C. T. Chan, and M. Xiao, *Nat. Rev. Phys.* **5**, 659 (2023).
- J. Wang, P. Li, X. Zhao, *et al.*, *Photonics Insights* **3**, R01 (2024).
- Y. Zeng, X. Zhang, X. Ouyang, *et al.*, *Adv. Opt. Mater.* **12**, 2400296 (2024).
- B. Zhen, C. W. Hsu, L. Lu, *et al.*, *Phys. Rev. Lett.* **113**, 257401 (2014).
- Y. Zhang, A. Chen, W. Liu, *et al.*, *Phys. Rev. Lett.* **120**, 186103 (2018).
- T. Zhang, K. Dong, J. Li, *et al.*, *Nat. Commun.* **14**, 6014 (2023).
- B. Wang, W. Liu, M. Zhao, *et al.*, *Nat. Photonics* **14**, 623 (2020).
- P. Huo, W. Chen, Z. Zhang, *et al.*, *Nat. Commun.* **15**, 3055 (2024).
- G. Sun, Y. Wang, Y. Li, *et al.*, *Phys. Rev. B* **109**, 035406 (2024).
- X. Zhang, J. Xu, and Z. Zhu, *Laser & Photonics Rev.* **19**, 2401138 (2025).
- M. V. Gorkunov, A. A. Antonov, and Y. S. Kivshar, *Phys. Rev. Lett.* **125**, 093903 (2020).
- Y. Chen, H. Deng, X. Sha, *et al.*, *Nature* **613**, 474 (2023).
- W. Liu, B. Wang, Y. Zhang, *et al.*, *Phys. Rev. Lett.* **123**, 116104 (2019).
- M. Kang, Z. Zhang, T. Wu, *et al.*, *Nat. Commun.* **13**, 4536 (2022).
- H. Qin, Z. Su, M. Liu, *et al.*, *Light. Sci. & Appl.* **12**, 66 (2023).
- L. Huang, W. Zhang, and X. Zhang, *Phys. Rev. Lett.* **128**, 253901 (2022).
- X. Ni, Y. Liu, B. Lou, *et al.*, *Phys. Rev. Lett.* **132**, 073804 (2024).
- J. Huang, G. Qing, D. Zhang, *et al.*, *Phys. Rev. B* **112**, 205421 (2025).
- E. Yao, Z. Su, Y. Bi, *et al.*, *J. Phys. D: Appl. Phys.* **57**, 375104 (2024).
- H. Luo, L. Liu, J. Zhang, *et al.*, *Opt. Express* **33**, 1703 (2025).
- Y. Ma, F. Deng, K. Ma, *et al.*, *J. Appl. Phys.* **138**, 053101 (2025).
- X. Zhao, J. Wang, W. Liu, *et al.*, *Phys. Rev. Lett.* **135**, 046203 (2025).
- C. Zhao, S. Dong, Q. Zhang, *et al.*, *Opt. Lett.* **47**, 2754 (2022).
- B. J. Zheng, W. J. Shi, H. Y. Dong, *et al.*, *Phys. Rev. Res.* **7**, 013091 (2025).
- S. Gao, T. Liu, S. Iwamoto, and Y. Ota, *ACS Photonics* **12**, 6745 (2025).
- W. Lv, H. Qin, Z. Su, *et al.*, *Sci. Adv.* **10**, eads0157 (2024).
- R. Zhang, X.-C. Li, and Q. H. Liu, *Phys. Rev. B* **112**, 014417 (2025).
- X. Zhao, J. Wang, W. Liu, *et al.*, *Phys. Rev. Lett.* **133**, 036201 (2024).
- Q.-A. Tu, H. Zhou, D. Zhao, *et al.*, *Photonics Res.* **12**, 2972 (2024).
- Y. Ma, F. Deng, K. Ma, *et al.*, *J. Appl. Phys.* **138**, 053101 (2025).
- J. Zak, E. R. Moog, C. Liu, and S. D. Bader, *Phys. Rev. B* **43**, 6423 (1991).